Journal of Sound and Vibration (1999) **226**(3), 549–571
Article No. jsvi.1999.2297, available online at http://www.idealibrary.com on IDEAL®

A COMPARATIVE STUDY OF FEEDFORWARD CONTROL OF HARMONIC AND RANDOM SOUND TRANSMISSION INTO AN ACOUSTIC ENCLOSURE

S. M. KIM AND M. J. BRENNAN

*Institute of Sound and Vibration Research, University of Southampton, Highfield, Southampton, S*017 1*BJ, England*

(*Received* 16 *December* 1998, *and in final form* 29 *March* 1999)

This paper describes an analytical and experimental investigation which compares the feedforward control of harmonic and random sound transmission into an acoustic cavity. A rectangular enclosure is considered that has five acoustically rigid walls and a flexible plate on the remaining side through which a plane acoustic wave is transmitted into the enclosure. The control systems are designed to reduce the acoustic potential energy inside the enclosure when the incident sound is either harmonic or random. Three control configurations classified by the type of actuators are investigated both theoretically and experimentally. They are (i) use of a single point-force actuator, (ii) use of a single acoustic piston source and (iii) simultaneous use of both a point-force actuator *and* an acoustic piston source. It is shown that the configuration of both acoustic and structural actuators is desirable for the active control of *both* harmonic and random sound transmission into a coupled structural–acoustic system whose response is governed by plate and cavity-controlled modes.

© 1999 Academic Press

1. INTRODUCTION

The active control of sound transmission into acoustic enclosures has been of interest in recent years because of increasing demands for a quieter environment [1]. One particular problem that has received much attention has been the active control of harmonic sound transmission into aircraft cabins. The noise source in this case is the propellers, and the noise has been controlled by loudspeakers inside the cabin [2], or structural actuators [3]. Numerous laboratory-scale studies have also been conducted on the active control of harmonic sound transmission into a cavity using structural actuators; see, for example, references [4–6]. Kim and Brennan [7, 8] undertook a recent study on a simple laboratory-scale system to investigate the use of *both* acoustic and structural actuators to control harmonic sound transmission into an acoustic cavity. They concluded that there was some merit in using a combination of structural and acoustic actuators.

The active control of random sound transmission into an enclosure is a more difficult problem. It has been studied by van den Dool *et al.* [9], who were

0022-460X/99/380549 + 23 $30.00/0 © 1999 Academic Press

interested in controlling the noise generated by rocket motors at launch, from being transmitted into the playload bay of the Ariane 5. They used either loudspeakers or PZT patches attached to the structure, and concluded that either system would work, but many structural actuators were required because of their limited output. Sampath and Balachandran [10] conducted a laboratory scale study on the control of random sound into an enclosure. They used a feedforward control strategy with PZT patches as the actuators and distributed PVDF structural sensors and a microphone as the error sensors. They found that better results were achieved when only the microphone was used as the error sensor.

The work presented here is a theoretical and experimental investigation into the feedforward active control of *random* sound transmission into a structural–acoustic coupled system by using both structural and acoustic actuators. To accomplish this task a multi-channel version of Wiener filter theory [11–13] is used. The results achieved for random sound are then compared with the results achieved for harmonic sound transmission using the same actuator configurations. The paper is organized as follows. Following the introduction, an analytical model is formulated in section 2, which leads to the simulations for a simple rectangular enclosure presented in section 3. The experimental work is reported in section 4, where off-line feedforward controllers for harmonic and random sound control are implemented using plant models identified from measurements. These results are compared with the predictions made by using the analytical model. Finally, the paper is closed with some conclusions in section 5. The appendix at the end describes the details of the analytical model for structural–acoustic coupled systems.

2. FEEDFORWARD CONTROL OF THE TRANSMISSION OF SOUND INTO AN ACOUSTIC ENCLOSURE

2.1. PHYSICAL SYSTEM MODELLING

Consider an enclosure surrounded by an acoustically rigid wall within which a flexible panel is fitted as shown in Figure 1. Three separate sets of co-ordinates are used to describe the system; co-ordinate $\mathbf{x}$ is used for the acoustic field in the cavity, co-ordinate $\mathbf{y}$ is used for the vibration of the structure, and co-ordinate $\mathbf{r}$ is used for the sound field outside the enclosure. An acoustic plane wave is incident on the flexible structure, and the aim of the active control system is to globally minimize the sound transmission through the flexible structure into the enclosure. Feedforward control is considered for both harmonic and random sound, and the differences between the control performances are investigated for both types of excitation when acoustic and structural actuators are used as secondary sources. A reference microphone can be seen outside the acoustic enclosure, and the pressure sensed by this transducer is denoted p_{mic}. This is used to measure the incident acoustic wave, and to provide a reference signal to drive both the acoustic source and the structural force actuator via the feedforward controllers, $H_q(\mathrm{j}\omega)$ and $H_f(\mathrm{j}\omega)$ respectively. In this section the theoretical framework to study this problem is formulated in the frequency domain.

Following the work of the control of harmonic sound transmission described by Kim and Brennan [7, 8], the time-averaged acoustic potential energy inside the cavity of volume V is adopted as the global measure of control performance and is given by [14, 15]

$$E_p = (V/4\rho_0 c_0^2)\ \mathbf{a}^{\mathrm{H}}\,\mathbf{a}, \tag{1}$$

where ρ_0 and c_0 denote the density and the speed of sound in air, respectively, and the acoustic modal amplitude vector $\mathbf{a}$ consists of the complex amplitudes of the acoustic pressure modes $a_n(\omega)$. Since N-number of acoustic modes are assumed to contribute to the acoustic pressure in the frequency range of interest, the vector $\mathbf{a}$ is of length N, and the superscript H denotes the Hermitian transpose.

The acoustic modal amplitude vector $\mathbf{a}$ has three contributions; the responses from the incident plane wave, the control force f_c, and the acoustic control source q_c and can be written as [7, 8]

$$\mathbf{a} = (\mathbf{I} + \mathbf{Z_a}\,\mathbf{Y_{cs}})^{-1}\ \mathbf{Z_a}\ (\mathbf{C}\mathbf{Y_s}\mathbf{g_p} + \mathbf{d_q}\,q_c + \mathbf{C}\mathbf{Y_s}\mathbf{d_f}\,f_c). \tag{2}$$

A derivation of this expression is presented for the general case of multiple acoustic and structural actuators in Appendix A. Since only a single acoustic actuator q_c and a single structural actuator f_c are considered, vectors $\mathbf{d_q}$ and $\mathbf{d_f}$ are used instead of matrices $\mathbf{D_q}$ and $\mathbf{D_f}$ in equation (A16) respectively. $\mathbf{Z_a}$ and $\mathbf{Y_s}$ are the uncoupled modal acoustic impedance and uncoupled modal structural mobility matrices respectively. The matrix $\mathbf{Y_{cs}}$ is the coupled modal structural mobility matrix and the matrix $\mathbf{C}$ is the structural–acoustic mode shape coupling matrix. The vector $\mathbf{g_p}$ is the generalized modal force vector due to the primary plane wave excitation which can be measured by the reference microphone denoted by p_{mic}. The N-length vector $\mathbf{d_q}$ determines the coupling between acoustic mode shapes and the location of the acoustic source at $\mathbf{x}_q$, whereas the M-length vector $\mathbf{d_f}$ determines the coupling between structural mode shapes and the location of the force actuator at $\mathbf{y}_f$. Substituting equation (2) into equation (1) gives the Hermitian quadratic form of complex variables q_c and f_c.

In practice, modal sensors that measure acoustic modal amplitudes are not available. An alternative approach is to use microphones to measure acoustic pressure fluctuations at a number of sensor locations, and then sum the squares of the pressure amplitudes measured at these locations to give an approximation to the acoustic potential energy. The approximation is given by [15]

$$\hat{E}_p = \frac{V}{4\rho_0 c_0^2 L} \sum_{l=1}^{L} |\,p(\mathbf{x}_l,\,\omega)\,|^2, \tag{3}$$

where $p(\mathbf{x}_l,\,\omega)$ is the complex pressure amplitude at the lth sensor location. Equation (3) can also be written as

$$\hat{E}_p = (V/4\rho_0 c_0^2 L)\ \mathbf{p}^{\mathrm{H}}\,\mathbf{p}, \tag{4}$$

where $\mathbf{p}$ is the L-length vector whose lth component is $p(\mathbf{x}_l,\,\omega)$, and is related to the modal amplitude vector $\mathbf{a}$ by

$$\mathbf{p} = \Psi_L^{\mathrm{T}}\,\mathbf{a}\,, \tag{5}$$

where the $(L \times N)$-size matrix Ψ_L^T contains the N modal amplitudes at L sensor locations. This can be substituted into equation (4) which also gives the Hermitian quadratic form of complex variables q_c and f_c. The solution which minimizes equation (4) gives the optimal control sources for control of a harmonic incident acoustic wave, which has been discussed by Kim and Brennan [7, 8].

2.2. CONTROL SYSTEM MODELLING

Instead of using the Hermitian quadratic form, in this paper, the classical Wiener filter theory is employed as an alternative approach. This is because the aim is to solve the achievable attenuation in sound transmission for a *spectrally white random* incident wave as well as for a *harmonic* incident wave. The Wiener filter, which results from the solution of Wiener–Hopf equation, is an optimal filter that offers the minimum mean-square error in a stationary random signal environment [11–13]. Kim [16] showed that the Wiener filter solutions with and without *the constraint of causality* offer the optimal controllers for *random* and *harmonic* sound fields respectively. Thus, in this section the theoretical model described in the previous section is reorganized in the time domin to apply the Wiener filter theory.

To set up the problem as a multiple-input–multiple-output (MIMO) Wiener filter problem, the feedforward controller can be drawn as a block diagram as shown in Figure 2(a). Two linear-time-invariant controllers $H_q(\mathrm{j}\omega)$ and $H_f(\mathrm{j}\omega)$ are used to control the secondary sources q_c and f_c in order to minimize the L-length error vector $\mathbf{p}$ in the mean square sense. The L-length vector $\boldsymbol{G}_p(\mathrm{j}\omega)$ denotes the primary plant frequency response function from the incident plane wave to the acoustic pressure vector $\mathbf{p}$, and $\boldsymbol{G}_q(\mathrm{j}\omega)$ and $\boldsymbol{G}_f(\mathrm{j}\omega)$ denote the secondary plant frequency response functions from the acoustic and structural actuators to the acoustic pressure vector $\mathbf{p}$ respectively. Because all systems are assumed to be linear time invariant, it can be redrawn as a 2-input L-output Wiener filter problem as shown in Figure 2(b), and the desired and received signal vectors can be written as

$$\boldsymbol{D}(\omega) = \boldsymbol{G}_p(\mathrm{j}\omega)\, p_{mic}, \qquad \boldsymbol{R}_q(\omega) = \boldsymbol{G}_q(\mathrm{j}\omega)\, p_{mic}, \qquad \boldsymbol{R}_f(\omega) = \boldsymbol{G}_f(\mathrm{j}\omega)\, p_{mic}, \quad \text{(6a–c)}$$

where from equations (2) and (5) the plant frequency response functions are $\boldsymbol{G}_p(\mathrm{j}\omega) = \boldsymbol{\Psi}_L^{\mathrm{T}}\,(\mathbf{I} + \mathbf{Z}_{\mathbf{a}}\,\mathbf{Y}_{\mathbf{cs}})^{-1}\,\mathbf{Z}_{\mathbf{s}}\mathbf{C}\mathbf{Y}_{\mathbf{s}}\,\mathbf{g}_{\mathbf{q}}/p_{mic}$, $\boldsymbol{G}_q(\mathrm{j}\omega) = \boldsymbol{\Psi}_L^{\mathrm{T}}\,(\mathbf{I} + \mathbf{Z}_{\mathbf{a}}\,\mathbf{Y}_{\mathbf{cs}})^{-1}\,\mathbf{Z}_{\mathbf{a}}\mathbf{d}_{\mathbf{q}}$ and $\boldsymbol{G}_f(\mathrm{j}\omega) = \boldsymbol{\Psi}_L^{\mathrm{T}}(\mathbf{I} + \mathbf{Z}_{\mathbf{a}}\,\mathbf{Y}_{\mathbf{cs}})^{-1}\,\mathbf{Z}_{\mathbf{a}}\mathbf{C}\mathbf{Y}_{\mathbf{s}}\mathbf{d}_{\mathbf{f}}$. It is useful to draw a time–domain version of Figure 2(b) so that standard techniques can be used to calculate the appropriate Wiener filters, and this is shown in Figure 2(c). The received signals and impulse responses of the Wiener filters can be expressed in vector–matrix form, and are given by

$$\boldsymbol{r}(t) = [\boldsymbol{r}_q(t) \qquad \boldsymbol{r}_f(t)], \qquad h(t) = \{h_q(t)\; h_f(t)\}^{\mathrm{T}}, \qquad \text{(7a, b)}$$

where the impulse response functions of the Wiener filters are $h_q(t) = \mathscr{F}^{-1}\{H_q(\omega)\}$, $h_f(t) = \mathscr{F}^{-1}\{H_f(\omega)\}$ where $\mathscr{F}^{-1}$ denotes the inverse Fourier transforms. The desired and received signal vectors can be obtained from the time–domain versions of equations (6a–c) as

$$\boldsymbol{d}(t) = \boldsymbol{g}_p(t) * p_{mic}(t), \qquad \boldsymbol{r}_q(t) = \boldsymbol{g}_q(t) * p_{mic}(t), \qquad \boldsymbol{r}_f(t) = \boldsymbol{g}_f(t) * p_{mic}(t), \quad \text{(8a–c)}$$

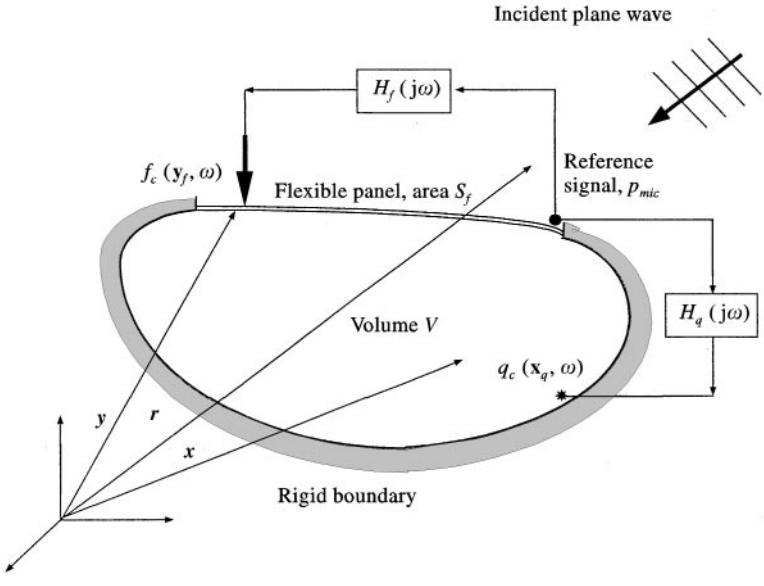

Figure 1. Feedforward control of sound transmission using both structural and acoustic actuators.

where the operator $*$ denotes the convolution integral, and the impulse response functions are obtained from the corresponding frequency response functions, i.e. $\boldsymbol{g}_p(t) = \mathscr{F}^{-1}\{\boldsymbol{G}_p(\omega)\}$, and $\boldsymbol{g}_q(t) = \mathscr{F}^{-1}\{\boldsymbol{G}_q(\omega)\}$, and $\boldsymbol{g}_f(t) = \mathscr{F}^{-1}\{\boldsymbol{G}_f(\omega)\}$. In addition, the L-length estimated signal vector is $\boldsymbol{y}(t) = \boldsymbol{r}(t) * \boldsymbol{h}(t)$.

Now the problem is to design the Wiener filters $h_q(t)$ and $h_f(t)$ which minimize the mean-square error $J = E[\boldsymbol{e}^{\mathrm{T}}(t)\boldsymbol{e}(t)]$ when the desired and received signals are stationary random. The operator $E[\cdot]$ denotes the ensemble average, and the error vector $\boldsymbol{e}(t) = \boldsymbol{d}(t) + \boldsymbol{y}(t)$ is measured with the L microphones inside the cavity. Thus, a direct relationship between the physical system in Figure 1 and the block diagram in Figure 2(c) which represents a 2-input-L-output Wiener filter problem has been established.

The optimal filters can be obtained by solving the Wiener–Hopf equations for the system shown in Figure 2(c). The Wiener–Hopf equations for the 2-input L-output system are an extension of the single-input–multiple-output case described by Nelson *et al.* [17], and are given by [16]

$$\int_0^\infty \left(h_{oq}(\tau_2) \sum_{l=1}^{L} R_{qq,l}(\tau_1 - \tau_2) + h_{of}(\tau_2) \sum_{l=1}^{L} R_{qf,l}(\tau_1 - \tau_2) \right) \mathrm{d}\tau_2 = -\sum_{l=1}^{L} R_{qd,l}(\tau_1), \quad \tau_1 \geqslant 0, \tag{9a}$$

$$\int_0^\infty \left(h_{oq}(\tau_2) \sum_{l=1}^{L} R_{fq,l}(\tau_1 - \tau_2) + h_{of}(\tau_2) \sum_{l=1}^{L} R_{ff,l}(\tau_1 - \tau_2) \right) \mathrm{d}\tau_2 = -\sum_{l=1}^{L} R_{fd,l}(\tau_1), \quad \tau_1 \geqslant 0. \tag{9b}$$

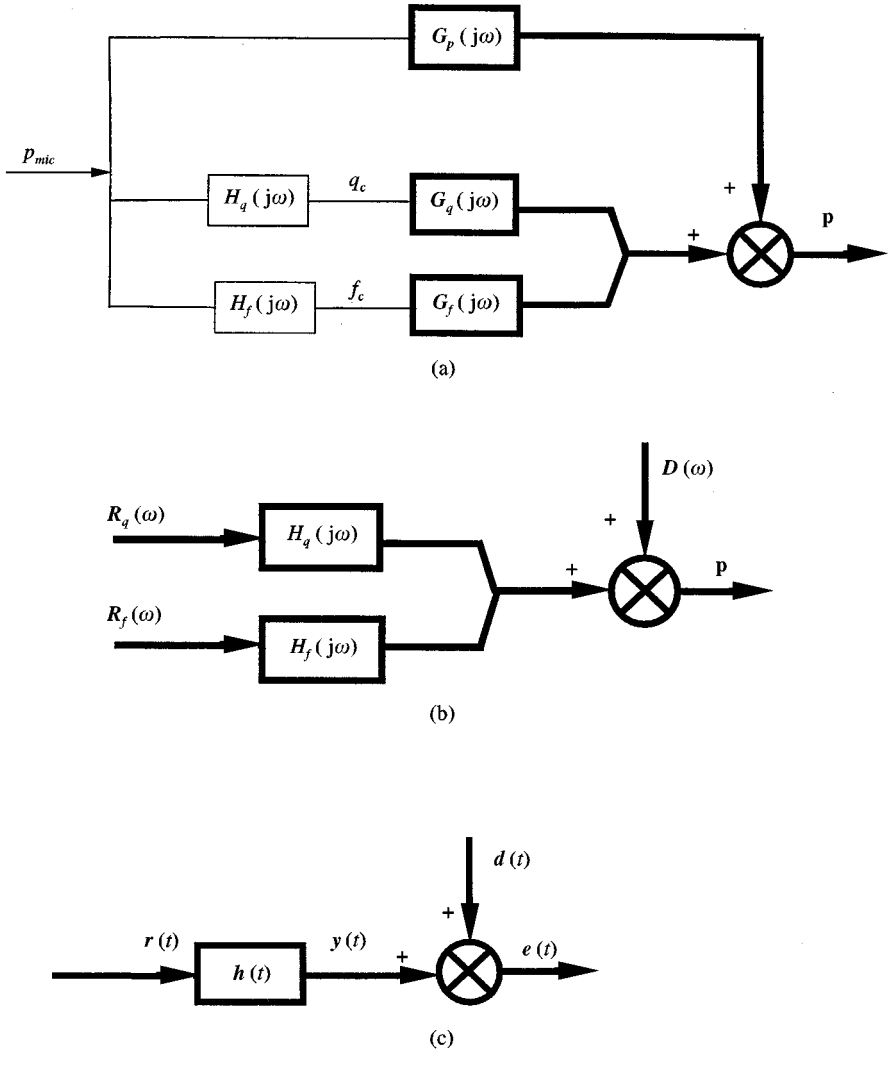

Figure 2. A block diagram of the feedforward control of sound transmission using both an acoustic and a structural actuator. (a) Feedforward control of sound transmission; (b) 2 input N output Wiener filter problem (frequency domain); (c) time–domain block diagram representation.

Note that the integral equations are subject to the constraint of causality $\tau_1 \geqslant 0$ and the filters are intrinsically constrained to be causal since $\tau_2 \geqslant 0$. The variables τ_1 and τ_2 are arbitrary time variables, $h_{oq}(\tau_2)$ and $h_{of}(\tau_2)$ are the impulse response functions of the optimal filters, and $R_{qq,l}(\tau) = E[r_{q,l}(t) r_{q,l}(t+\tau)]$ and $R_{ff,l}(\tau) = E[r_{f,l}(t) r_{f,l}(t+\tau)]$ are the respective autocorrelation functions of the received signals at the lth filter block. $R_{qf,l}(\tau) = E[r_{q,l}(t) r_{f,l}(t+\tau)]$, $R_{fq,l}(\tau) = E[r_{f,l}(t) r_{q,l}(t+\tau)]$, $R_{qd,l}(\tau) = E[r_{q,l}(t) d_l(t+\tau)]$ and $R_{fd,l}(\tau) = E[r_{f,l}(t) d_l(t+\tau)]$ are cross-correlation functions. When the optimal filters are implemented, the *minimum* mean-square error is given by [16]

$$J_0 = \sum_{l=1}^{L} R_{dd,l}(0) + \int_0^{\infty} \left(h_{oq}(\tau_1) \sum_{l=1}^{L} R_{qd,l}(\tau_l) + h_{of}(\tau_1) \sum_{l=1}^{L} R_{fd,l}(\tau_1) \right) \mathrm{d}\tau_1 \quad (10)$$

which can be normalized by the mean-square error without control $\sum_{l=1}^{L} R_{dd,l}(0)$ to give

$$J'_o = 1 + \frac{\int_0^\infty \left(h_{oq}\ (\tau_1) \sum_{l=1}^{L} R_{qd,l}\ (\tau_1) + h_{of}\ (\tau_1) \sum_{l=1}^{L} R_{fd,l}\ (\tau_1) \right) \mathrm{d}\tau_1}{\sum_{l=1}^{L} R_{dd,l}\ (0)}. \quad (11)$$

When the incident wave in Figure 1 is a harmonic acoustic wave, the optimal controllers can be easily obtained by solving the Wiener–Hopf equation, equation (9), without the constraint of causality [16]. In this case, the desired and received signals are harmonic, and the solution for this case will be described in section 2.3. When a random acoustic wave is incident, the optimal controllers are the solution of equation (9). In general, however the Wiener–Hopf equation in the continuous time–domain either does not have an analytic solution as a closed form or is very complicate to solve. In this paper (section 2.4), thus the discrete time–domain version is considered, which does have a closed-orm solution. This is also advantageous when digital filters are implemented.

2.3. CONTROL OF HARMONIC SOUND

When designing an optimal controller for harmonic sound, the constraints of causality in equation (9) can be relaxed. Thus the simple Fourier transforms of equations (9a, b) can be written in matrix–vector form as

$$\boldsymbol{A}(\omega)\boldsymbol{H}_{uo}\ (\mathrm{j}\omega) = -\boldsymbol{b}(\omega), \quad (12)$$

where $\boldsymbol{H}_{uo}\ (\mathrm{j}\omega)$ is the unconstrained Wiener filter, and the input spectrum matrix $\boldsymbol{A}(\omega)$ is Herimitian and is given by

$$\boldsymbol{A}(\omega) = \sum_{l=1}^{L} \begin{bmatrix} S_{qq,l}(\omega) & S_{qf,l}(\omega) \\ S_{fq,l}(\omega) & S_{ff,l}(\omega) \end{bmatrix}, \quad (13)$$

and the elements of the matrix are $S_{qq,l}(\omega) = E\,[R^*_{q,l}(\omega)R_{q,l}(\omega)]$, $S_{qf,l}(\omega) = E\,[R^*_{q,l}(\omega)R_{f,l}(\omega)]$, $S_{fq,l}(\omega) = E\,[R^*_{f,l}(\omega)R_{q,l}(\omega)]$ and $S_{ff,l}(\omega) = E\,[R^*_{f,l}(\omega)R_{f,l}(\omega)]$ where the superscript * denotes the complex conjugate. The unconstrained Wiener filter vector and the cross-spectrum vector are given by

$$\boldsymbol{H}_{uo}(\mathrm{j}\omega) = \begin{Bmatrix} H_{uoq}\ (\mathrm{j}\omega) \\ H_{uof}\ (\mathrm{j}\omega) \end{Bmatrix}, \qquad \boldsymbol{b}\,(\omega) = \sum_{l=1}^{L} \begin{Bmatrix} S_{qd,l}\ (\omega) \\ S_{fd,l}\,(\omega) \end{Bmatrix}, \quad (14a, b)$$

where $H_{uoq}\,(\mathrm{j}\omega)$ and $H_{uof}\ (\mathrm{j}\omega)$ are the unconstrained Wiener filters for the acoustic and structural actuators, respectively, and $S_{qd,l}(\omega) = E\,[R^*_{q,l}\,(\omega)D_l(\omega)]$ and $S_{fd,l}(\omega) = E\,[R^*_{f,l}\,(\omega)\,D_l(\omega)]$. If only one rather than two actuators is used, matrix $\boldsymbol{A}(\omega)$ becomes either $\boldsymbol{A}(\omega) = \sum_{l=1}^{L} [S_{qq\,,l}]$ for the acoustic actuator or $\boldsymbol{A}(\omega) = \sum_{l=1}^{L} [S_{ff\,,l}]$ for the structural actuator. Note if all systems and signals are deterministic,

the averaging process $E[\cdot]$ can be omitted. Equation (12) can be rearranged to give the unconstrained Wiener filter

$$\boldsymbol{H}_{uo}(\mathrm{j}\omega) = -\boldsymbol{A}^{-1}(\omega)\boldsymbol{b}(\omega). \tag{15}$$

The optimal source strength of actuators q_c and f_c can be obtained from the relationships $H_{uoq}(\mathrm{j}\omega) = q_c/p_{mic}$ and $H_{uof}(\mathrm{j}\omega) = f_c/p_{mic}$ respectively. The normalized minimum mean-square error can be written similarly as equation (11) as

$$J'_o(\omega) = 1 + \left(\boldsymbol{b}^{\mathrm{H}}(\omega)\boldsymbol{H}_{uo}(\omega)/\textstyle\sum_{l=1}^{L} S_{dd,l}(\omega)\right), \tag{16}$$

where the denominator $\sum_{l=1}^{L} S_{dd,l}(\omega)$ is the mean-square error without control. By using equation (15) it can be rewritten as

$$J'_o(\omega) = 1 - \left(\boldsymbol{b}^{\mathrm{H}}(\omega)\boldsymbol{A}^{-1}(\omega)\boldsymbol{b}(\omega)/\textstyle\sum_{l=1}^{L} S_{dd,l}(\omega)\right). \tag{17}$$

Equations (15) and (17) offer the optimal controllers and the normalized minimum of the approximation of the time-averaged acoustic potential energy for the case of a harmonic incident wave respectively.

2.4. CONTROL OF RANDOM SOUND

When white noise is incident on the plate, the digital optimal controllers can be obtained by solving the discrete forms of equations (9a, b) which can be written as

$$\sum_{i=0}^{I-1}\sum_{l=1}^{L} h_{oq}(i)\,R_{qq,l}(n-i) + h_{of}(i)\,R_{qf,l}(n-i) = -\sum_{l=1}^{L} R_{qd,l}(n), \quad n \geqslant 0, \tag{18a}$$

$$\sum_{i=0}^{I-1}\sum_{l=1}^{L} h_{oq}(i)\,R_{fq,l}(n-i) + h_{of}(i)\,R_{ff,l}(n-i) = -\sum_{l=1}^{L} R_{fd,l}(n), \quad n \geqslant 0, \tag{18b}$$

where I is the length of the finite impulse response (FIR) Wiener filters. Equations (18a, b) can be rewritten in vector–matrix form as

$$\boldsymbol{A}\boldsymbol{h}_{\mathrm{o}} = -\boldsymbol{b}, \tag{19}$$

where the input correlation matrix $\boldsymbol{A}$ is given by

$$\boldsymbol{A} = \sum_{l=1}^{L}\begin{bmatrix}\boldsymbol{A}_{qq,l} & \boldsymbol{A}_{qf,l}\\ \boldsymbol{A}_{fq,l} & \boldsymbol{A}_{ff,l}\end{bmatrix}, \tag{20}$$

which is a matrix consisting of sub-matrices that can be expressed as, for example,

$$\boldsymbol{A}_{qf,l} = \begin{bmatrix} R_{qf,l}(0) & R_{qf,l}(1) & \cdots & R_{qf,l}(I-1)\\ R_{qf,l}(-1) & R_{qf,l}(0) & \cdots & R_{qf,l}(I-2)\\ \vdots & \vdots & & \vdots\\ R_{qf,l}(-I+1) & R_{qf,l}(-I+2) & \cdots & R_{qf,l}(0)\end{bmatrix}, \tag{21}$$

where $R_{qf,l}(i) = E[r_{q,l}(l)\, r_{f,l}(l+i)]$. Although the element matrix $\boldsymbol{A}_{qf,l}$ itself is not symmetric because $R_{qf,l}(i) \neq R_{qf,l}(-i)$, it should be noted that the whole matrix $\boldsymbol{A}$ is symmetric because $\boldsymbol{A}_{qf} = \boldsymbol{A}_{fq}^{\mathrm{T}}$. The impulse response functions of the plants $\boldsymbol{g}_p(t)$, $\boldsymbol{g}_q(t)$ and $\boldsymbol{g}_f(t)$ given in equations (8a–c) are assumed to be modelled by J-length FIR filters. The $(2I)$-length column vectors are given by

$$\boldsymbol{h}_0 = \begin{Bmatrix} \boldsymbol{h}_{oq} \\ \boldsymbol{h}_{of} \end{Bmatrix}, \qquad \boldsymbol{b} = \sum_{l=1}^{L} \begin{Bmatrix} \boldsymbol{b}_{qd,l} \\ \boldsymbol{b}_{fd,l} \end{Bmatrix}, \tag{22a, b}$$

where for example, $\boldsymbol{h}_{oq} = \{h_{oq}(0)\ h_{oq}(1) \quad \cdots \quad h_{oq}(I-1)\}^{\mathrm{T}}$ and $\boldsymbol{b}_{qd,l} = \{R_{qd,l}(0)\ R_{qd,l}(1)\ \cdots\ R_{qd,l}(I-1)\}^{\mathrm{T}}$ where $R_{qd,l}(i) = E[r_{q,l}(l)\, d_l(l+i)]$. If only one rather than two actuators is used, the matrix $\boldsymbol{A}$ becomes either $\boldsymbol{A} = \sum_{l=1}^{L} [\boldsymbol{A}_{qq,l}]$ for the acoustic actuator or $\boldsymbol{A} = \sum_{l=1}^{L} [\boldsymbol{A}_{ff,l}]$ for the structural actuator. The matrix in this case again becomes real and symmetric.

The causally constrained Wiener filter can be determined by rearranging equation (19) to give

$$\boldsymbol{h}_0 = -\boldsymbol{A}^{-1}\, \boldsymbol{b} \tag{23}$$

and the discrete form of the normalized *minimum* mean-square error in equation (11) can be written similarly as equation (17) as

$$J_0' = 1 - \left(\boldsymbol{b}^{\mathrm{T}} \boldsymbol{A}^{-1}\, \boldsymbol{b} / \sum_{l=1}^{L} R_{dd,l}(0) \right). \tag{24}$$

If the incident acoustic plane wave is *white noise*, one can equivalently replace it by *an impulse* as far as the classical Wiener filter theory is concerned [13, 16]. In other words, the control problem for the white noise incident wave is equivalently transformed to active control of sound transmission for an impulsive incident wave. The advantage of this approach is much less numerical computations, since it significantly shortens the time consuming convolution and correlation processes involved with random signal inputs as in equations (8) and (18). In the simulations in this paper, white noise is replaced by an impulse for p_{mic} in equation (8). Due to the replacement an easier deterministic and systematic approach can be used to the stochastic optimal control problem.

3. SIMULATIONS

To compare the control performances for harmonic and random sound discussed in section 2, a duct-like rectangular enclosure is considered that has five rigid walls and a simply supported flexible plate on the top as shown in Figure 3. This behaved as a one-dimensional wave system in the low frequency range, and was chosen for the convenience of analysis and experimental work, without loss of generality of the physics of sound transmission. Three co-ordinates systems, **x**, **y**, **r** are used to specify the cavity, the plate and the external sound field respectively. The flexible aluminium plate is assumed to be fitted in an infinite baffle, which is not shown for clarity. The dimensions of the cavity are $L_1 \times L_2 \times L_3$ where $L_1 = 1{\cdot}5$ m, $L_2 = 0{\cdot}3$ m, and $L_3 = 0{\cdot}4$ m, and the thickness of the plate is 5 mm. A plane wave is

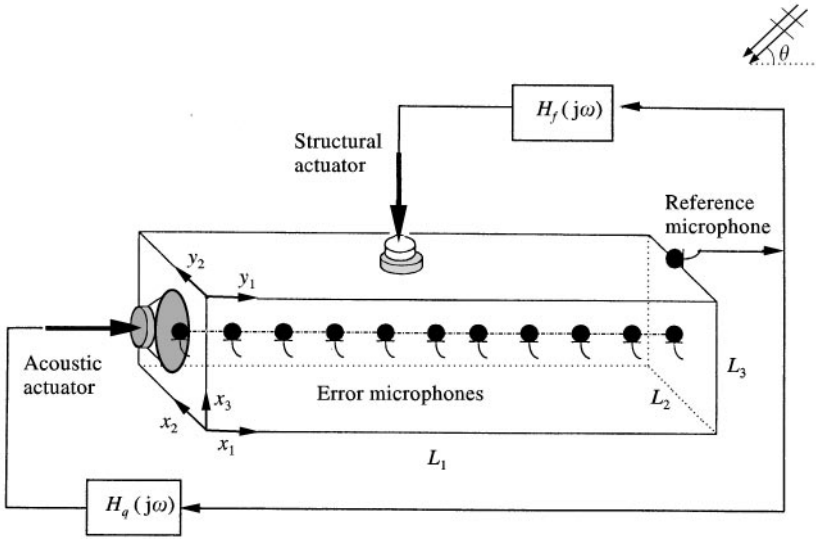

Figure 3. Feedforward control of sound transmission into a rectangular enclosure.

TABLE 1

Material properties of materials used in the simulations and experimental work

Material	Density (kg/m^3)	Phase speed (m/s)	Young's modulus (N/m^2)	Poisson's ratio (ν)	Damping ratio (ζ)
Air	1·21	340	—	—	0·01
Al	2770	—	71×10^9	0·33	0·01

assumed to be incident on the plate with angles of ($\varphi = 0^\circ$) and ($\theta = 45^\circ$) where φ is the angle from the co-ordinate y_1 on the plate and θ is the angle of incidence from the plate. The incident wave is measured with the reference microphone located at the right-hand edge of the plate and its signal is used to drive both the acoustic and structural actuators via the controllers $H_q(j\omega)$ and $H_f(j\omega)$ respectively.

The approximated acoustic potential energy, which is the measure of control performance as discussed in section 2, is measured by using the 11 equally spaced microphones along the centre line of the duct. The acoustic control source is a loudspeaker of radius 0·15 m which is fitted at the left end with its centre at (0, $L_2/2$, $L_3/2$), and a point force located at ($9L_1/20$, $L_2/2$) on the plate is used as the structural actuator. The material properties of air and aluminium (A1) used in this simulations are listed in Table 1. The modal damping ratios of the plate and the cavity were assumed to be 0·01, and the time constant of the first acoustic mode was taken to be 0·2 s. A total of four acoustic and six structural modes were assumed to contribute to the coupled responses within the frequency range of interest. Table 2 shows the natural frequencies of the uncoupled structural and acoustic systems and their geometric mode shape coupling coefficients normalized by their

TABLE 2

Natural frequencies and geometric mode-shape coupling coefficients of the uncoupled structural and acoustic systems

Order		Plate	1	2	3	4	5	6
	Type		(1,1)	(2,1)	(3,1)	(4,1)	(5,1)	(6,1)
Cavity		Freq. (Hz)	141	157	184	222	270	330
1	(0,0,0)	0	1·00	0	0·33	0	0·20	0
2	(1,0,0)	113	0	0·94	0	0·38	0	0·24
3	(2,0,0)	227	− 0·47	0	0·81	0	0·34	0
4	(3,0,0)	340	0	− 0·57	0	0·81	0	0·31

maximum value. (m_1, m_2) and (n_1, n_2, n_3) indicate the indices of the mth plate mode and the nth cavity mode. Plant responses were calculated up to 512 Hz with a frequency interval of 0·5 Hz. Modes above 340 Hz were excluded from the simulations in order to reduce numerical errors involved with inverse Fourier transform calculations. Reasonably correct predictions at low frequencies under 340 Hz were considered sufficient to investigate control mechanisms.

Three control configurations, classified by the type of actuators are investigated both theoretically and experimentally. They are (i) use of a single point-force actuator, (ii) use of a single acoustic piston source, and (iii) simultaneous use of both a point-force actuator *and* an acoustic piston source.

Before considering the control of random sound it is instructive to review the behaviour of the control system for harmonic sound. This has been discussed in detail for the three control configurations in references [7, 8]. The acoustic potential energy with and without control is calculated by using the procedure in section 2.3. They are shown in Figure 4(a) for the acoustic actuator alone, Figure 4(b) for the structural actuator alone, and Figure 4(c) for both acoustic and structural actuators. The signs "$*$" and "$\circ$" denote the uncoupled structural and acoustic natural frequencies respectively. As discussed by Kim and Brennan [7, 8], the acoustic actuator is effective in controlling the acoustic potential energy at frequencies where cavity-controlled modes dominate the acoustic response of the cavity. Whereas, the structural actuator is effective in controlling the acoustic potential energy at frequencies where plate-controlled modes dominated the response. It can be seen in Figure 4(c) that the simultaneous use of both actuators results in very good control of sound transmission into the enclosure. Kim has shown that the simultaneous use of both structural and acoustic actuators to control harmonic sound transmission into a structural–acoustic coupled system offers the best performance with the least number of actuators [16].

For the control of the white noise incident wave, the procedure described in section 2.4 is used to determine the optimal Wiener filters for the three actuator configurations. Minimization of the acoustic potential energy using the acoustic actuator is considered first. Figure 5(a) shows the acoustic potential energy with

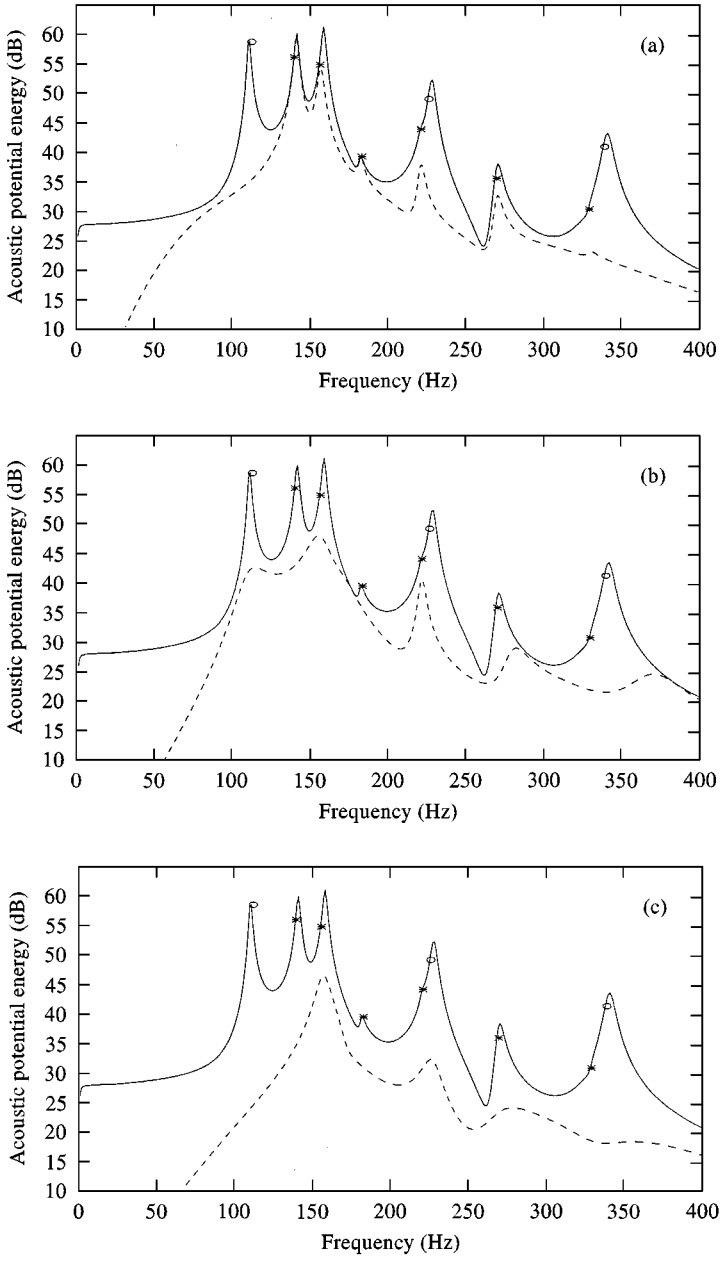

Figure 4. Predicted acoustic potential energy without (solid line) and with control according to the actuators used (dashed). The signs "$*$" and "$\circ$" denote the uncoupled structural and acoustic natural frequencies respectively. (a) Acoustic actuator used; (b) structural actuator used; (c) simultaneous use of both acoustic and structural actuators.

and without control. The solid line is the acoustic potential energy without control, and the potential energies with control are shown for both random (dashed) and harmonic (dotted) sound for comparison. The constrained Wiener filter is a 400-coefficient FIR filter and its response is shown in Figure 5(b). As stated

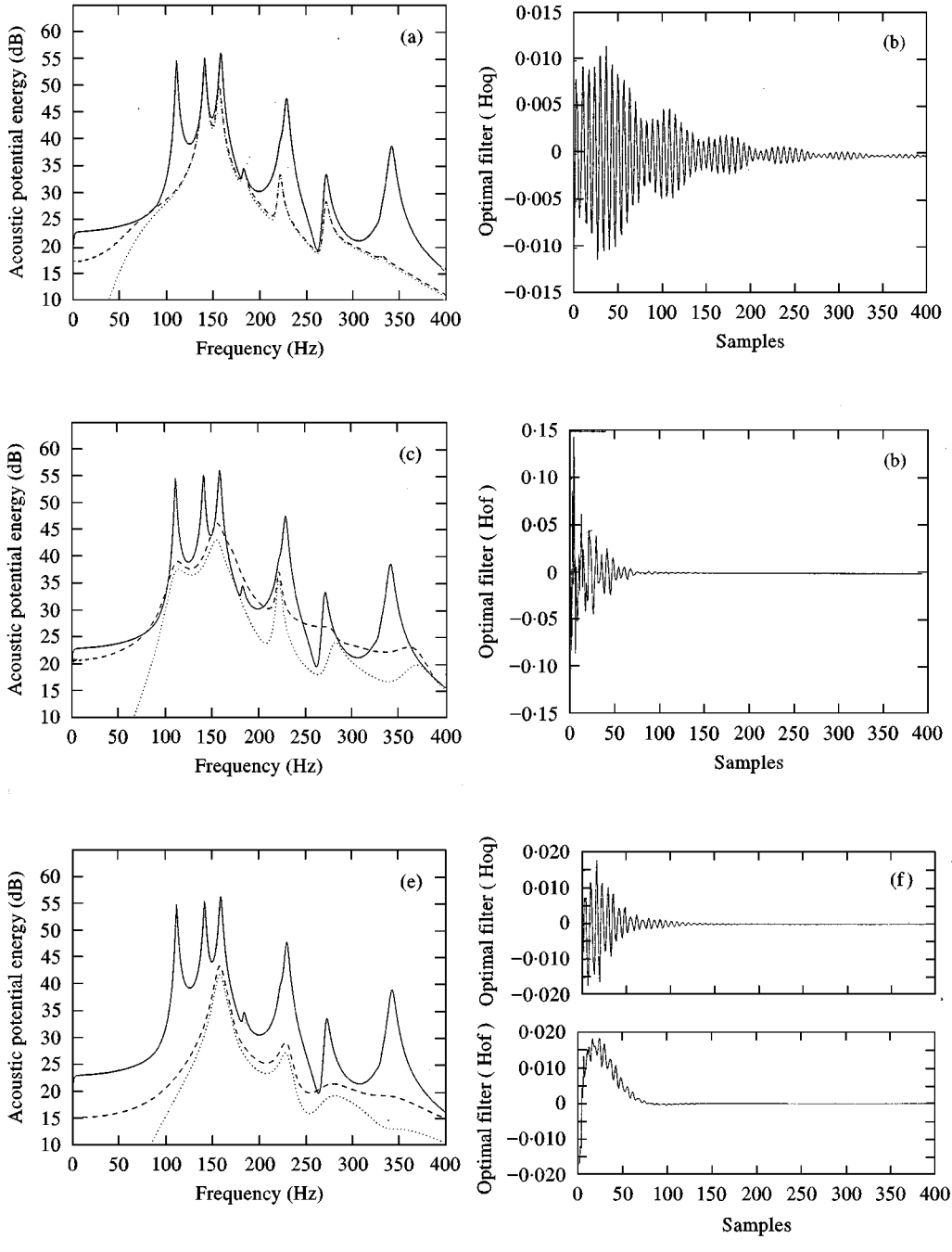

Figure 5. Predicted control performance with optimal constrained and unconstrained feedforward controllers on the attenuation of sound transmission into the rectangular enclosure shown in Figure 3. Acoustic potential energy without control (solid), acoustic potential with constrained (dash) and unconstrained (dotted) optimal controllers. (a) Acoustic potential energy with and without control; the acoustic actuator is the secondary source; (b) impulse response of the constrained optimal controller with an acoustic secondary source; (c) acoustic potential energy with and without control; the structural actuator is the secondary source; (d) impulse response of the constrained optimal controller with a structural secondary source; (e) acoustic potential energy with and without control; both acoustic and structural actuators are used as secondary sources. (f) impulse response of the constrained optimal controllers; acoustic (upper), structural (lower).

TABLE 3

Comparison of control performances according to the use of the actuators (*simulation*)

Use of the actuators	Energy ratio J_o' (%)		Overall reduction J_o' (dB)	
	Harmonic	Random	Harmonic	Random
Acoustic source	39·13	42·94	− 4·1	− 3·7
Point force	13·16	26·69	− 8·8	− 5·7
Both actuators	4·6	7·0	− 13·4	− 11·5

earlier, the random and harmonic sound controllers are the casually constrained and unconstrained optimal Wiener filters respectively. It can be seen that control performance for harmonic sound is better than that for random sound at all frequencies, but there is very little difference at frequencies greater than about 100 Hz. Overall performances of each controller in terms of the normalized mean-square error calculated by using equations (17) and (24) are tabulated in Table 3. It can be seen that there is only a small overall performance difference between the harmonic and random noise cases.

Figure 5(c) shows the control performance when the structural actuator is used as the secondary source, and Figure 5(d) shows the impulse response of the constrained Wiener filter. Examination of Figure 5(c) shows, that although the harmonic controller reduces the acoustic potential energy at all frequencies, the random controller does not. The energy is reduced considerably at resonance frequencies, where there is an increase in the predictability of the cost function, but there is an increase in the potential energy at other frequencies. The overall control performance is shown in Table 3. There is a difference of about 3·1 dB between harmonic and random sound excitation for the structural actuator, and this should be compared with the performance difference of about 0·4 dB for the acoustic actuator. This is because the wave propagation delays from the structural actuator to acoustic responses measured by the microphones are larger than those from the acoustic actuator. Control performance of the feedforward controllers for random sound depends mainly upon the time taken for the incident wave to travel from the reference microphone to the error microphones via the secondary actuators. In the application discussed here, it takes longer for the structural actuator, rather than the acoustic actuator, to control the error microphone responses. Since the physical system is dispersive [18], it can be more precisely investigated by examining the *phase angle difference* between the desired signal set and the received signal set [16].

When both acoustic and structural actuators are used, the potential energy with and without control is shown in Figure 5(e), and the impulse responses of the optimal filters are shown in Figure 5(f). It is clear that the control performance with both actuators is far superior to that when individual actuators are used, even when the excitation is random. By examining Figures 5(b), (d) and (f), it can be seen that the controllers are quite different in the configuration where both actuators are used. A striking difference is that the impulse response of the controller for the

acoustic actuator becomes much shorter in Figure 5(f). This is probably because the structural actuator is controlling the low frequencies in the case. As can be seen from Table 3, a reduction in the mean-square response of over 10 dB for both harmonic and random sound cases is achieved for the lightly damped system considered. Thus, it has been demonstrated that the control performance of the hybrid system for both harmonic and random sound is superior to that when the actuators are used separately. In addition, when both actuators are used the performance difference between harmonic and random sound cases is not appreciable.

4. EXPERIMENTAL WORK

To validate the analytical model and to check the predicted characteristics of the control systems discussed above, some experiments were performed on a system similar to that shown in Figure 3. A photograph of the experimental set-up is shown in Figure 6(a). This shows an elevated large loudspeaker that generates the acoustic incident wave, which then excites the aluminium plate fitted inside a wooden baffle. The speaker was positioned about 2 m from the right-hand edge of the plate and was facing down at an angle of approximately 45°. In Figure 6(b), the reference microphone measuring the incident wave can be seen close to the right-hand edge of the plate. The AVC Instrumentation Series 712 inertial piezoelectric actuator with a proof mass of 150 g, which was used as the point force control actuator, can also be seen in the central area of the plate. The duct-like rectangular enclosure was constructed with the same dimensions of the simulation model considered in the last section (the cavity had dimensions of $L_1 \times L_2 \times L_3$ where $L_1 = 1{\cdot}5$ m, $L_2 = 0{\cdot}3$ m, and $L_3 = 0{\cdot}4$ m, and the thickness of aluminium plate was 5 mm). The control speaker was fitted into the left-hand face of the enclosure as shown in Figure 3. To make the acoustically rigid boundary conditions, the wooden walls were made of 25 mm thick plywood and were surrounded by 75 mm deep sand layers packed by an extra container as shown in Figure 6(c). A simply supported boundary condition for the plate was fabricated with 1·25 mm thick steel strips bolted along the edge of the plate as shown in Figure 6(d). The design concept relies upon the fact that the thin strip is relatively rigid to in-plane motion but is flexible to rotation.

The main purpose of the experimental work was to identify the system impulse responses of the primary and secondary plants. Off-line optimal control of harmonic and random sound transmission could then be performed using the identified plant impulse response functions in a similar way to the procedure used in the simulations presented in the previous section. Note however in the previous section the impulse responses were obtained from the direct inverse Fourier transforms of the avilable plant frequency response functions. A single moving microphone was used to measure the sound response at 11 equi-distance positions along the duct-like enclosure. The primary plant was identified by using signals from the error microphone at 11 positions inside the cavity and the signal from the reference microphone when the system was excited with the elevated loudspeaker outside the cavity. The acoustic and structural secondary plants were identified by

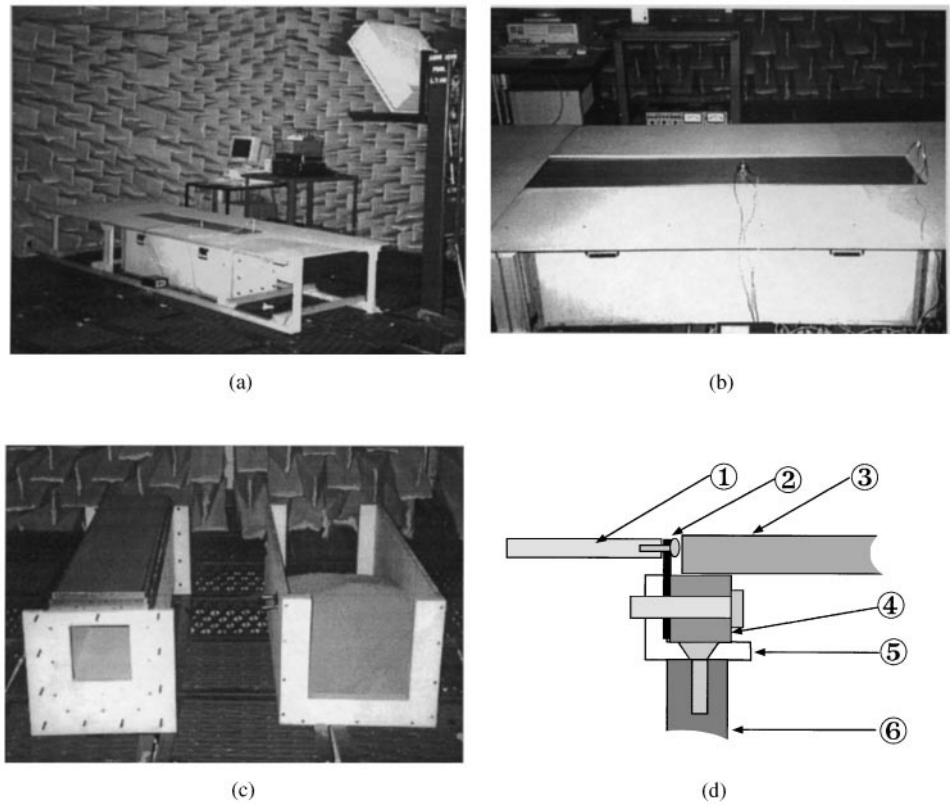

Figure 6. Experimental set-up; (a) General arrangement; (b) side-view showing the secondary actuator (centre of plate) and reference microphone (right-hand side of plate); (c) experimental set-up disassembled showing the outer casing and the insulating sand; (d) diagram showing the plate-fixing arrangements; ① A1 plate 5 mm, ② steel strip, ③ Baffle, ④ Adapter (steel), ⑤ aluminium angle, and ⑥ 25 mm plywood.

using the error microphone responses at the 11 positions to the input signals of the control speaker and the force actuator, respectively. A low-passed version of random noise was used to excite the three actuators for the system identification of the primary and secondary plants. The merits of using this type of signal actuation were that higher acoustic modes were not excited, and the aliasing error on sampling was minimized.

A finite impulse response (FIR) filter of 1024 coefficients was used to model the impulse response of each plant. Since the mean-square error was adopted as the criterion of modelling performance, the identification of each plant was a single-input–single-output Wiener filter problem. General discussions on system identification problems are available in the literaure; see, for example, reference [19]. Both excitation and error microphone signals were measured simultaneously for each plant over a 40 s period with the sampling frequency 1024 Hz so that each had 40 960 data points. In the identification of $\boldsymbol{G}_q(\omega)$ the derivative of source strength was used rather than the source strength as this was directly measurable using an accelerometer attached to the speaker. Long-length filters were required

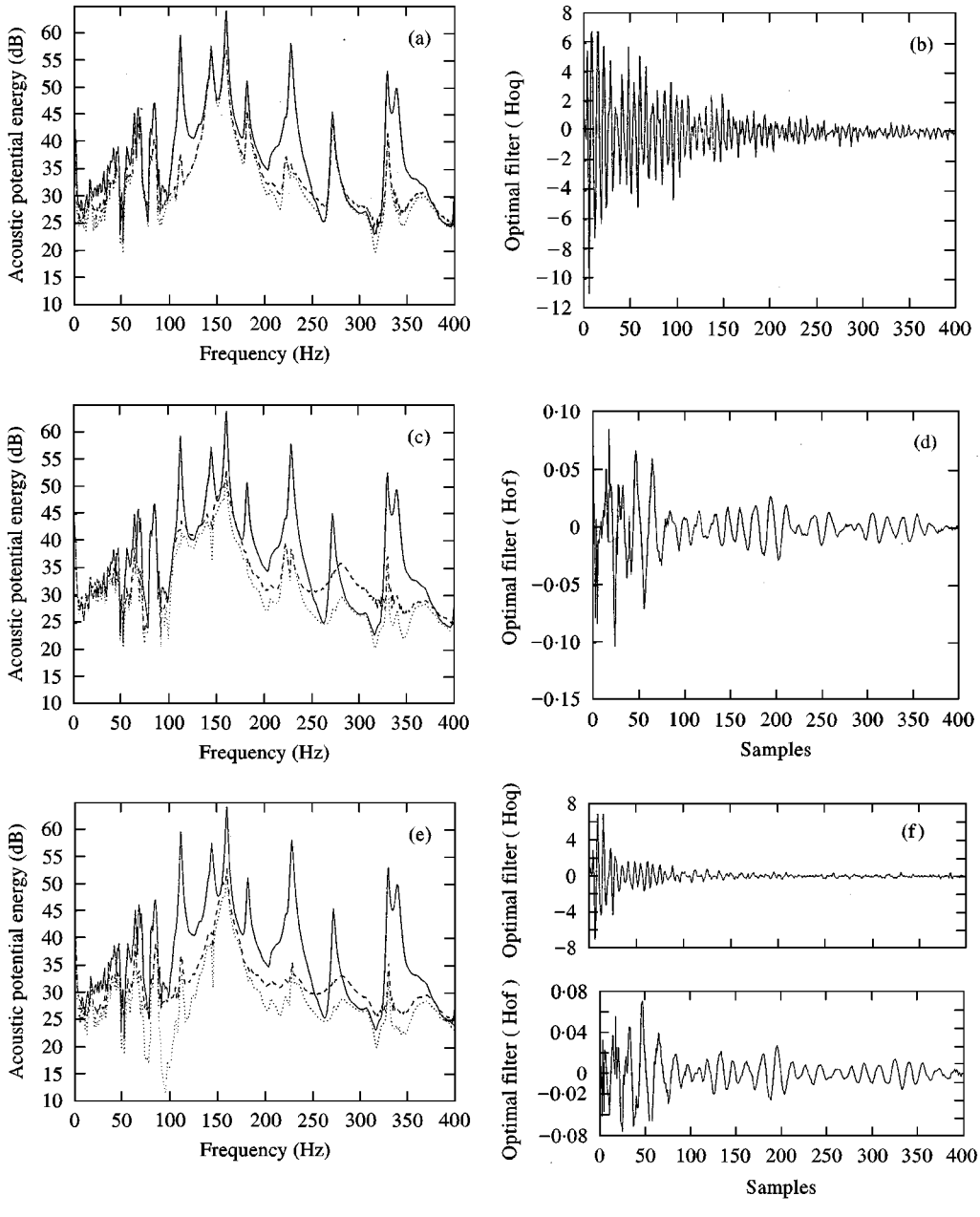

Figure 7. Experimental control performance with optimal constrained and unconstrained feedforward controllers on the attenuation of sound transmission into the rectangular enclosure shown in Figure 3. Acoustic potential energy without control (solid), acoustic potential with constrained (dash) and unconstrained (dotted) optimal controllers. (a) Acoustic potential energy with and without control; the acoustic actuators is the secondary sources; (b) impulse response of the constrained optimal controller with an acoustic secondary source; (c) acoustic potential energy with and without control; the structural actuator is the secondary source; (d) impulse response of the constrained optimal controller with a structural secondary source; (e) acoustic potential energy with and without control; both acoustic and structural actuators are used as secondary sources; (f) impulse response of the constrained optimal controllers; acoustic (upper), structural (lower).

because the systems were lightly damped. However, this imposes a heavy computational burden since the identification method involves matrix inversion of a large input auto-correlation matrix. Although this was not an issue in the off-line control system considered in this work, if real time control is to be implemented then an alternative method would be to use infinite-impulse-response (IIR) filters using an auto-regressive-moving-average (ARMA) model as discussed by Vipperman *et al.* [20]. Accurate modelling with error values less than 1% was achieved for most primary and secondary plants. In general, poor coherence between the input excitation and output response signals causes large modelling errors.

By using the impulse responses identified from the experiment, the theoretical optimal control models developed in section 2 were used. The control performance results are presented in Figure 7, which has the same format as Figure 5 so that the experimental results can be compared easily with the predictions. It can be seen that below about 100 Hz the measured results are contaminated by noise due to low-sensitivity between the external reference and internal error microphones. At high fequencies, the differences between the experimental results and the predictions was due to the practical difficulty of generating a plane wave with a fixed incident angle.

Examination of Figures 7(a) and 7(c) shows that, as predicted, the acoustic actuator is effective in controlling harmonic sound at frequencies close to the cavity-controlled modes (113, 227·5 and 339 Hz), and the structural actuator is effective in controlling harmonic sound at plate-controlled modes (143, 160, 180·5 271 and 328·5 Hz). As predicted, by using both actuators better control performance can be achieved at all frequencies which can clearly be seen in Figure 7(e). Some differences in the predicted and experimetnal impulse response functions for the controllers are thought to be because of the poorly correlated measured responses at low frequencies.

A general observation is that the experimental results are largely as predicted by the analytical model for all three actuator configurations, and for both random and harmonic sound control. The overall control performances are tabulated in Table 4. It can be seen that the use of both types of actuators offers a better performance than the separate use of each actuator in both harmonic and random sound fields.

TABLE 4

Comparison of control performances according to the use of the actuators (*experiment*)

Use of the actuators	Energy ratio J'_o (%)		Overall reduction J'_o (dB)	
	Harmonic	Random	Harmonic	Random
Acoustic source	30·25	33·63	− 5·2	− 4·7
Point force	13·58	21·18	− 8·7	− 6·7
Both actuators	7·93	12·18	− 11·0	− 9·1

5. CONCLUSIONS

The active control of random sound transmission through a flexible plate into an acoustic enclosure has been considered, and its control performance has been compared with that for the active control of harmonic sound transmission. In particular, the role of acoustic and structural actuators for the control of harmonic and random sound has been investigated. A theoretical model to design optimal controllers for harmonic and random sound has been presented using the theoretical basis of the Wiener filter. The theoretical model is based on two fundamental facts. Firstly, the Weiner filters with and without the constraint of causality are the optimal controllers of stationary random sound and harmonic sound, respectively. Secondary, as far as Wiener filter design is concerned, white noise is equivalently replaced by an impulse. By using these facts, a systematic and deterministic approach has been applied to design optimal controllers for harmonic and random sound waves when they are transmitted to a duck-like rectangular acoustic enclosure.

Both theoretical and experimental results obtained demonstrate that in harmonic sound control, the acoustic actuator is effective in controlling cavity-controlled modes while the structural actuator is effective in controlling plate-controlled modes. In random sound control, the acoustic actuator achieves reductions similar to that for the control performance for harmonic sound, but reductions achieved by the structural actuator are diminished. This is because the wave propagation delays from the acoustic actuator to the acoustic responses measured by error microphones are smaller than those from the structural actuator. From the simulations and experimental results it can be concluded that the hybrid configuration of both acoustic and structural actuators is advantageous for the active control of *both* harmonic and random sound transmission into a structural-acoustic coupled system whose response is governed by plate- and cavity-controlled modes.

REFERENCES

1. S. J. Elliott and P. A. Nelson 1994 *Noise/News International*, *June* 75–97. Active noise control.
2. S. J. Eliott, P. A. Nelson, I. M. Stothers and C. C. Boucher 1990 *Journal of Sound and Vibration* **140**, 219–238. In-flight experiments on the active control of propeller induce cabin noise.
3. C. R. Fuller and J. D. Jones 1987 *Journal of Sound and Vibration* **112**, 389–395. Experiments on reduction of propeller induced interior noise by active control of cylinder vibration.
4. S. D. Snyder and N. Tanaka 1993 *Journal of the Acoustical Society of America* **94**, 2181–2193. On feedforward active control of sound and vibration using vibration error signals.
5. J. Pan, C. H. Hansen and D. A. Bies 1990 *Journal of the Acoustical Society of America* **87**, 2098–2108. Active control of noise transmission through a panel into a cavity: I. Analytical study.
6. J. Pan, C. H. Hansen 1991 *Journal of the Acoustical Society of America* **90**, 1488–1501. Active control of noise transmission through a panel into a cavity: II. Experimental study.

7. S. M. Kim and M. J. Brennan 1997 *Proceedings of the Sixth International Conference on Recent Advances in Structural Dynamics, Southampton, England*, 14–17 *July*, Vol 2, 1233–1246. Active control of sound transmission into a rectangular enclosure using both structural and acoustic actuators.
8. S. M. Kim and M. J. Brennan 1998 *Journal of the Acoustical Society of America*. Active control of harmonic sound transmission into an acoustic enclosure using both structural and acoustic actuators (submitted).
9. T. Van Den Dool, N. Doelman, S. Hausler and H. Baier 1997 *Proceedings of Active* 97, *Budapest, Hungary*, 21–23 *August* Broadband MIMO in an Ariane fairing model.
10. A. Sampath amd B. Balachandran 1996 *Proceedings of the ASME Conference, Atlanta, Georgia* 17–22 *November* 1996, AD-Vol 52, 479–484. Active control of transmission of band-limited disturbances into a three-dimensional enclosure.
11. N. Wiener 1950 *Extrapolation, Interpolation, and Smoothing of Stationary Time Series*. The Technology Press of the Massachusettes Institute of Technology, New York: Wiley.
12. A. Papoulis 1984 *Signal Analysis*. New York: McGraw-Hill International Editions.
13. H. L. Van Trees 1968 *Detection, Estimation, and Modulation Theory Part I*. New York: Wiley.
14. E. H. Dowell, G. F. Gorman, III and D. A. Smith 1977 *Journal of Sound and Vibration* **52**, 519–542. Acoustoelasticity: general theory, acoustic modes and forces response to sinusoidal excitation, including comparisons with experiment.
15. A. J. Bullmore, P. A. Nelson, A. R. D. Curtis and S. J. Elliott 1987 *Journal of Sound and Vibration* **117**, 15–33. The active minimization of harmonic enclosed sound fields, Part II: a computer simulation.
16. S. M. Kim 1998 *Ph.D. Thesis, University of Southampton*. Active control of sound in structural-acoustic coupled systems.
17. P. A. Nelson, J. K. Hammond, P. Joseph, and S. J. Elliott 1990 *Journal of the Acoustical Society of America* **87**, 963–975. Active control of stationary random sound fields.
18. L. Cremer and M. Heckl 1987 *Structure-Borne Sound: Structural Vibrations and Sound Radiation at Audio Frequencies*. Berlin: Springer-Verlag. Second edition.
19. L. Ljung 1987 *System Identification: Theory for the User*. Englewood Cliffs NJ: Prentice-Hall INC.
20. J. S. Vipperman, R. A. Burdisso and C. R. Fuller 1993 *Journal of the Acoustical Society of America* **166**, 283–299. Active control of broadband structural vibration using the LMS adaptive algorithm.
21. F. J. Fahy 1985 *Sound and Structural Vibration, Radiation, Transmission and Response*. London: Academic Press.
22. S. M. Kim and M. J. Brennan 1999 *Journal of Sound and Vibration* **223**, 97–113. A compact matrix formulation using the impedance and mobility approach for the analysis of structural-acoustic systems.

APPENDIX A: DERIVATION OF THE ANALYTICAL MODEL OF THE STRUCTURAL-ACOUSTIC SYSTEM

The aim in this appendix is to describe the analytical model of the structural–acoustic system shown in Figure 1. A harmonic plane wave is assumed to be incident on the flexible structure, and wave interference outside the enclosure between the incident and radiated waves by structural vibration is neglected. If the acoustic pressure and the structural vibration are assumed to be described by a summation of N and M modes, respectively, then the acoustic pressure at position

x inside the enclosure and the structural vibration velocity at position **y** are given by

$$p(\mathbf{x}, \omega) = \sum_{n=1}^{N} \psi_n(\mathbf{x})\, a_n(\omega) = \mathbf{\Psi}^{\mathrm{T}} \mathbf{a}, \qquad u(\mathbf{y}, \omega) = \sum_{m=1}^{M} \phi_m(\mathbf{y})\, b_m(\omega) = \mathbf{\Phi}^{\mathrm{T}} \mathbf{b}, \qquad \text{(A1, A2)}$$

where the N length column vectors $\mathbf{\Psi}$ and $\mathbf{a}$ consist of the array of uncoupled acoustic mode shape functions $\psi_n(\mathbf{x})$ and the complex amplitude of the acoustic pressure modes $a_n(\omega)$ respectively. Likewise the M length column vectors $\mathbf{\Phi}$ and $\mathbf{b}$ consist of the array of uncoupled vibration mode shape functions $\phi_m(\mathbf{y})$ and the complex amplitude of the vibration velocity modes $b_m(\omega)$ respectively.

The mode shape functions $\psi_n(\mathbf{x})$ and $\phi_m(\mathbf{y})$ satisfy the orthogonal property in each uncoupled system, and are normalized as follows:

$$V = \int_V \psi_n^2(\mathbf{x})\, \mathrm{d}V, \qquad S_f = \int_{S_f} \phi_m^2(\mathbf{y})\, \mathrm{d}S, \qquad \text{(A3, A4)}$$

where V and S_f are the volume of the enclosure and the area of the flexible plate, respectively. The complex amplitude of the nth acoustic mode under structural and acoustic excitation is given by [14]

$$a_n(\omega) = \frac{\rho_o c_0^2}{V} A_n(\omega) \left(\int_V \psi_n(\mathbf{x})\, s(\mathbf{x}, \omega) \mathrm{d}V + \int_{S_f} \psi_n(\mathbf{y})\, u(\mathbf{y}, \omega) \mathrm{d}S \right), \qquad \text{(A5)}$$

where $s(\mathbf{x}, \omega)$ denotes the acoustic source strength density function in the cavity volume V, and $u(\mathbf{y}, \omega)$ denotes the normal velocity of the flexible plate of area S_f. The two integrals inside the brackets represent the nth acoustic modal source strength contributed from $s(\mathbf{x}, \omega)$ and $u(\mathbf{y}, \omega)$ respectively. The acoustic mode resonance term $A_n(\omega)$ is given by

$$A_1(\omega) = \frac{1}{1/T_a + \mathrm{j}\omega} \quad \text{when } n = 1,$$

$$A_n(\omega) = \frac{\mathrm{j}\omega}{\omega_n^2 - \omega^2 + \mathrm{j}\, 2\, \zeta_n \omega_n \omega} \quad \text{when } n \neq 1, \qquad \text{(A6a, b)}$$

where T_a is the time constant of the first acoustic mode, and ω_n and ζ_n are the natural frequency and damping ratio of the nth acoustic mode respectively. Substituting equation (A2) into equation (A5) and introducing the modal source strength $q_n = \int_V \psi_n(\mathbf{x}) s(\mathbf{x}, \omega) \mathrm{d}V$, one obtains

$$a_n(\omega) = \frac{\rho_o c_0^2}{V} A_n(\omega) \left(q_n(\omega) + \sum_{m=1}^{M} C_{n,m}\, b_m(\omega) \right), \qquad \text{(A7)}$$

where $C_{n,m}$ represents the geometric coupling relationship between the uncoupled structural and acoustic mode shape functions on the surface of the vibrating structure S_f and is given by [21]

$$C_{n,m} = \int_{S_f} \psi_n(\mathbf{y}) \phi_m(\mathbf{y}) \mathrm{d}S. \qquad \text{(A8)}$$

If one uses L independent acoustic control sources, q_n can be written as

$$q_n(\omega) = \sum_{l=1}^{L} \frac{1}{S_{q,l}} \int_V \psi_n(\mathbf{x}_{c,l})\, \mathrm{d}V q_{c,l}(\omega) = \sum_{l=1}^{L} D_{q,nl}\, q_{c,l}(\omega), \tag{A9}$$

where $D_{q,nl} = (1/S_{q,l}) \int_V \psi_n(\mathbf{x}_{c,l})\mathrm{d}V$, and the lth control source strength $q_{c,l}(\omega)$ having an area of $S_{q,l}$ is defined at $\mathbf{x}_{c,l}$. Thus, the complex amplitude of the acoustic modal pressure vector $\mathbf{a}$ can be expressed as

$$\mathbf{a} = \mathbf{Z}_\mathbf{a}(\mathbf{D}_\mathbf{q}\mathbf{q}_\mathbf{c} + \mathbf{C}\mathbf{b}), \tag{A10}$$

where $\mathbf{Z}_\mathbf{a} = (\rho_0 c_0^2/V)\,\mathbf{A}$ is the *uncoupled acoustic modal impedance matrix*, which determines the relationship between the acoustic source excitation and the resultant acoustic pressure in modal co-ordinates of the uncoupled acoustic system [22]. The matrix $\mathbf{A}$ is a $(N \times N)$ diagonal matrix in which each (n, n) diagonal term consists of A_n, the $(N \times M)$ matrix $\mathbf{C}$ is the structural–acoustic mode shape coupling matrix, the $(N \times L)$ matrix $\mathbf{D}_\mathbf{q}$ determines coupling between the L acoustic source locations and the N acoustic modes, the L length vector $\mathbf{q}_\mathbf{c}$ is the complex strength vector of acoustic control sources, and $\mathbf{b}$ is the complex vibration modal amplitude vector.

If one assumes that the flexible structure is an isotropic plate, the complex vibration velocity amplitude of the mth mode can be expressed as [14]

$$b_m(\omega) = \frac{1}{\rho_s h S_f} B_m(\omega) \left(\int_{S_f} \phi_m(\mathbf{y})\,(f(\mathbf{y}, \omega) + p^{ext}(\mathbf{y}, \omega) - p(\mathbf{y}, \omega))\mathrm{d}S \right), \tag{A11}$$

where again ρ_s is the density of the plate material, h is the thickness, and S_f is the area of the plate. Inside the integral $f(\mathbf{y}, \omega)$, $p^{ext}(\mathbf{y}, \omega)$, and $p(\mathbf{y}, \omega)$ denote the force distribution function, and the exterior and interior acoustic pressure distributions on the surface S_f, respectively. The exterior pressure $p^{ext}(\mathbf{y}, \omega)$ is measured by the reference microphone denoted by p_{mic} in Figure 1. Because of the sign convention used, there is a minus sign is front of $p(\mathbf{y}, \omega)$. The structural mode resonance term $B_m(\omega)$ can be expressed as

$$B_m(\omega) = \frac{\mathrm{j}\omega}{\omega_m^2 - \omega^2 + \mathrm{j}2\zeta_m \omega_m \omega}, \tag{A12}$$

where ω_m and ζ_m are the natural frequency and the damping ratio of mth mode respectively. Substituting equation (A1) into equation (A11), one obtains

$$b_m(\omega) = \frac{1}{\rho_s h S_f} B_m(\omega) \left(g_{c,m}(\omega) + g_{p,m}(\omega) - \sum_{n=1}^{N} C_{n,m}^{\mathrm{T}}\, a_n(\omega) \right), \tag{A13}$$

where $g_{c,m}(\omega) = \int_{S_f} \phi_m(\mathbf{y}) f(\mathbf{y}, \omega)\mathrm{d}S$, $g_{p,m}(\omega) = \int_{S_f} \phi_m(\mathbf{y})\, p^{ext}(\mathbf{y}, \omega)\, \mathrm{d}S$, and $C_{n,m}^{\mathrm{T}} = C_{m,n}$. If one uses K independent point force actuators, the mth mode generalized force due to control forces, $g_{c,m}$, can be written as

$$g_{c,m}(\omega) = \sum_{k=1}^{K} \int_{S_f} \phi_m(\mathbf{y})\, \delta(\mathbf{y} - \mathbf{y}_{c,k})\mathrm{d}S f_{c,k}(\omega) = \sum_{k=1}^{K} D_{f,mk} f_{c,k}(\omega), \tag{A14}$$

where $D_{f,mk} = \int_{S_f} \phi_m(\mathbf{y})\,\delta(\mathbf{y} - \mathbf{y}_{c,k})\mathrm{d}S$, and the kth control point force $f_{c,k}(\omega)$ is located at $\mathbf{y}_{c,k}$. Thus the modal vibration amplitude vector $\mathbf{b}$ can be expressed as

$$\mathbf{b} = \mathbf{Y}_s\,(\mathbf{g}_p + \mathbf{D}_f\,\mathbf{f}_c - \mathbf{C}^T\,\mathbf{a}), \tag{A15}$$

where $\mathbf{Y}_s = (1/\rho_s h S_f)\ \mathbf{B}$ is the *uncoupled structural modal mobility matrix* which determines the relationship between structural excitation and the resultant structural velocity response in modal co-ordinates of the uncoupled structural system [22]. The matrix $\mathbf{B}$ is a $(M \times M)$ diagonal matrix in which each (m, m) diagonal term consists of B_m, $\mathbf{C}^T$ is the transpose matrix of $\mathbf{C}$, the $(N \times K)$ matrix $\mathbf{D}_f$ determines coupling between the K point force locations and the M structural modes, $\mathbf{g}_p$ is the generalized modal force vector due to the primary plane wave excitation, the K length vector $\mathbf{f}_c$ is the complex vector of structural control point forces, and $\mathbf{a}$ is the complex acoustic modal amplitude vector.

Combining equations (A10) and (A15), one obtains the acoustic modal amplitude vector for the coupled system

$$\mathbf{a} = (\mathbf{I} + \mathbf{Z}_a\,\mathbf{Y}_{cs})^{-1}\,\mathbf{Z}_a\,(\mathbf{C}\mathbf{Y}_s\,\mathbf{g}_p + \mathbf{D}_q\,\mathbf{q}_c + \mathbf{C}\mathbf{Y}_s\,\mathbf{D}_f\,\mathbf{f}_c), \tag{A16}$$

where $\mathbf{Y}_{cs} = \mathbf{C}\mathbf{Y}_s\,\mathbf{C}^T$ is defined as the *coupled structural modal mobility matrix* [22].